Enhanced Phase Realignment Techniques for the PAPR Reduction in OFDM Systems

Robin Shrestha, Jae Moung Kim, *Senior Member, IEEE*, and Jong-Soo Seo, *Fellow, IEEE*

***Abstract*—This paper presents a simple and effective solution for the peak-to-average power ratio (PAPR) problem in orthogonal frequency-division multiplexing (OFDM) systems. Since the OFDM signal has a high PAPR, it generates inevitable nonlinear distortions at the output of a high-power amplifier. A new technique of PAPR reduction called phase realignment (PR) and its modified version called modified PR (MPR) are proposed, which require neither side information nor do they impose any modification of the receiver. Furthermore, four possible variations of the MPR constellation structure are proposed and evaluated in terms of PAPR reduction and bit-error-rate (BER) performance. The proposed PR and MPR provide considerable reductions in PAPR. MPR_1 gives a comparatively high PAPR reduction, followed by MPR_3, PR, MPR_2, and MPR_4 in descending order. The PAPR reductions of MPR_3 and MPR_2 tend to converge to that of the PR as the modulation order increases, whereas MPR_4 gives a low PAPR reduction. These techniques are designed to allow a certain level of BER degradation, which is defined by a transmit error vector magnitude (EVM) limited to a specified threshold, to reduce the PAPR and the average power (equally important in terms of power efficiency). The proposed techniques produce the reduced out-of-band radiation compared with the original OFDM signal and have moderate computational complexity. The EVM threshold is imposed to design optimum amplitude and phase margins for the PR and MPRs. Furthermore, we present the analytic upper bound BER expressions of the proposed techniques.**

***Index Terms*—Bit error rate (BER), error vector magnitude (EVM), modified phase realignment (MPR), orthogonal frequency-division multiplexing (OFDM), peak-to-average power ratio (PAPR), phase realignment (PR).**

I. Introduction

THE peak-to-average power ratio (PAPR) problem is severe in orthogonal frequency-division multiplexing (OFDM) systems [1] due to the superposition of multiple signals in a time domain, which, in turn, requires the use of a highly linear high-power amplifier (HPA). The nonlinearity of the HPA generates both in-band distortion, which is responsible for the intersymbol interference, and out-of-band (OOB) radiations, which are responsible for the adjacent channel interference [2]. Consequently, the power efficiency becomes very poor without the application of the HPA nonlinearity mitigation technique.

Various PAPR reduction techniques have been proposed to include techniques based on signal distortion [3]–[6], signal scrambling [7]–[10], and coding [11]. An extended form of signal distortion is constellation shaping [12]–[17]. The work in [18] presents the detailed survey and analysis of some of the highly discussed PAPR reduction techniques.

These PAPR reduction techniques have their own pros and cons, be it in terms of bandwidth efficiency, system complexity, or loss of critical signal. Clipping is the simplest among them, but degrades the bit-error-rate (BER) performance and causes OOB noise [3]. Clipping and filtering (CF) would reduce the OOB radiation, but it causes some peak regrowth, which eventually exceeds the clipping level. Iterative clipping and filtering (ICF) [4] prevents the peak regrowth by repeating the CF operation to reach a discrete amplitude at the cost of additional complexity (proportional to the number of repetitions). All of these CF-based methods degrade the BER performance in spite of their high PAPR reduction capabilities. Windowing allows multiplying the large signal peaks with a specific window function, but there is always a tradeoff between OOB radiation and BER performance. Peak cancelation [5] produces smaller OOB radiation compared with the CF, and it leads to a better PAPR reduction without the loss of BER performance [6] at the expense of an overhead of a reference signal.

Signal scrambling is the probabilistic method for the PAPR reduction. Partial transmit sequence (PTS) [7], [8] and selective mapping (SLM) [9] have been mostly discussed in the scrambling method. Typically, this method introduces complexity to the system with a longer processing time and may require the side information to be transmitted. With the overhead information, tone reservation [10] achieves PAPR reduction depending on the number of reserved tones, their location in the frequency domain, and the optimization of their location [18]. The coding method [11] usually gives the worst case guarantee on the PAPR performance with some redundancy. There are also coding techniques that reduce the PAPR by using a special forward error correction code set, where the error probability depends on the power of a number of consecutive symbols rather than on an individual symbol [1].

The PAPR reduction based on CF noise shaping [13], [14] and constellation shaping [15]–[17] has also been proposed. Active constellation extension (ACE) dynamically extends the outer constellation points in the active channels to reduce the

Manuscript received January 28, 2015; revised May 21, 2015, July 23, 2015, and August 31, 2015; accepted September 26, 2015. Date of publication October 7, 2015; date of current version September 15, 2016. This work was supported in part by the Institute of BioMed-IT, Energy-IT, and Smart-IT Technology (BEST), a Brain Korea 21 plus program, Yonsei University, and in part by the ICT R&D program of MSIP/IITP (A Study on the Next-Generation Interactive Terrestrial Broadcasting System) under Grant 1391202006. The review of this paper was coordinated by Dr. J.-C. Chen. (*Corresponding author: Jong-Soo Seo.*)

R. Shrestha and J.-S. Seo are with the Department of Electrical and Electronic Engineering, Yonsei University, Seoul 120-749, Korea (e-mail: robinsth@yonsei.ac.kr; jsseo@yonsei.ac.kr).

J. M. Kim is with the Department of Information and Communication Engineering, Inha University, Incheon 402-751, Korea (e-mail: jaekim@inha.ac.kr).

Color versions of one or more of the figures in this paper are available online at http://ieeexplore.ieee.org.

Digital Object Identifier 10.1109/TVT.2015.2487992

peak margin without degrading the BER performance [13] at the cost of increased average power. In [14], constrained clipping for PAPR reduction is proposed, where the clipping noise is constrained based on the predefined threshold. However, the constraint appears to have no use upon optimizing the clipping level. The integer-based constellation shaping method [15] proposes an encoding of a cubic constellation called the Hadamard constellation, whose decision boundary runs along the bases defined by the Hadamard matrix in a transform domain. The amplitude and sign adjustment method [16] refines the constellation for PAPR reduction by adjusting the sign and amplitude of each subcarrier. The results in [16] show a high PAPR reduction with the amplitude and sign adjustment at the cost of increased average power by around 5%. A signal set expansion technique to reduce the PAPR of an OFDM signal is presented in [17], which has the drawback of increased power or BER degradation.

As reviewed, those techniques with the better PAPR reduction have either complexity issues or overhead transmission issues. The ACE is one of the techniques with the best tradeoff between performance and complexity, which has been adopted in DVB-T2 for the PAPR reduction [19]. One problem with the ACE is that it increases the average power of the OFDM signal, which is undesirable in terms of energy efficiency. We propose a PAPR reduction technique called the phase realignment (PR) [12], which gives a considerable PAPR reduction with decreased average power. In this paper, we extend our previous work [12] and propose a new technique of PAPR reduction called modified phase realignment (MPR). Furthermore, we generalize the proposed MPR technique for the higher order modulation (HOM) and propose four possible variations in the MPR constellation structure for M-ary quadrature amplitude modulation (M-QAM) with $M >= 16$. The four variations of the MPR structure are extensively studied via simulation. While the proposed techniques can also be effective in reducing the PAPR of the OFDM M-ary phase-shift keying (M-PSK) system, in this paper, we consider only the OFDM M-QAM system.

Similar to ACE, PR modifies the constellation points over the data subcarriers of the CF OFDM signal in the frequency domain. In PR, the phase of the CF constellation is restored back to its original phase, and the amplitude is limited within a specific amplitude margin from the amplitude of the conventional M-QAM constellation points. In MPR, a phase margin is introduced in addition to the amplitude margin. The phase of a CF constellation point beyond the allowable phase margin is restored to the respective phase threshold defined by the phase margin. The amplitude and phase margins are optimized to balance the tradeoff between PAPR reduction and BER degradation. The shortcoming of the PR and MPR is an acceptable degradation in BER performance, which is determined by limiting the transmit error vector magnitude (EVM) to a specified threshold. The effect of the EVM allowed in the PR/MPR would be minimized due to the effect of the PAPR reduction on the HPA [23].

The rest of this paper is organized as follows: Section II describes the OFDM system model considered in this paper and presents the PAPR and BER metrics along with the description of the HPA model. In Section III, we present the proposed PR and MPR techniques in detail and extend the MPR to four possible constellation structures. We also discuss the issue of the amplitude and the phase margin optimization and present the analysis of the computational complexity of the PR and MPR. In Section IV, we present the theoretical upper-bound BER of the PR and MPR. In Section V, we evaluate the performance of the proposed techniques and compare them with other existing techniques. Finally, in Section VI, we present the concluding remarks.

II. Orthogonal Frequency-Division Multiplexing System Model

We consider a typical OFDM system with N subcarriers. The OFDM system takes a set of input data bits $\mathbf{a} = [a_1 a_2, \ldots, a_{N \log_2 M}]$, which are modeled using the M-QAM to map into the I/Q channel baseband symbol X_n. N such modulated symbols, i.e., $(X_1, X_2, \ldots, X_N)$, are packed together to form N subcarriers at the input of the oversampling and inverse fast Fourier transform (IFFT) block using a serial-to-parallel converter.

The oversampled discrete-time OFDM signal $\mathbf{x} = [x_0 x_1, \ldots, x_{NL-1}]$ is generated by the IFFT operation as follows:

$$x_n = \frac{1}{\sqrt{NL}} \sum_{k=0}^{NL-1} X_n e^{\frac{j2\pi kn}{NL}} \ \forall\, n \in [0, 1, \ldots, NL-1] \quad (1)$$

where L is the oversampling factor that is large enough ($L \geq 4$) to better approximate the PAPR of x_n to that of the continuous-time OFDM signal. Here, we discuss some important theories related to the evaluation of a PAPR reduction technique.

A. PAPR Metric

N is considered to be very large, and according to the central limit theorem, the amplitude of an OFDM signal has a Rayleigh distribution [1]. The PAPR is generally used to describe the fluctuation of an OFDM signal. The PAPR per OFDM symbol can be obtained by

$$\text{PAPR} = \frac{\max\limits_{0 \leq n \leq NL-1} |x_n|^2}{\mathbb{E}\left[|\mathbf{x}|^2\right]} \quad (2)$$

where $\mathbb{E}[\bullet]$ denotes the expectation operator.

The PAPR reduction capability may be evaluated by using the complementary cumulative distribution function (CCDF). The CCDF is defined as the probability that the PAPR of an OFDM signal exceeds a given threshold Γ and is given by

$$\text{CCDF[PAPR]} = \Pr[\text{PAPR} > \Gamma]. \quad (3)$$

B. Power Amplifier Model

The high PAPR of an OFDM signal requires a highly linear transmission of the signal. HPAs are typically the most power-hungry components of radio frequency (RF) transceivers.

The power amplifier typically used for terrestrial and mobile communication is a solid-state power amplifier (SSPA). The

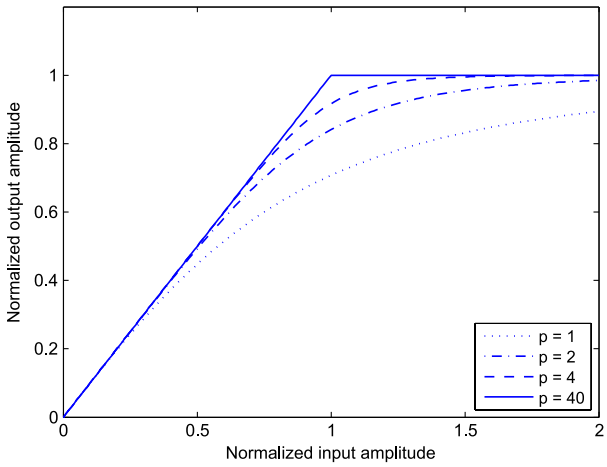

Fig. 1. AM/AM curves for the SSPA (Rapp's model) for different values of p.

complex RF output, which is nonlinearly distorted, can be expressed as

$$\begin{aligned} y(t) &= A\left(\rho(t)\right) e^{j\{\phi(t)+\Phi(\rho(t))\}} \\ &= Y\left(\rho(t)\right) e^{j\phi(t)} \end{aligned} \tag{4}$$

where $\rho(t)$ and $\phi(t)$ are the amplitude and phase of the input signal. $A(\bullet)$ and $\Phi(\bullet)$ are the AM/AM and the AM/PM conversion of the nonlinear distortion, respectively, and $Y(\rho(t)) = A(\rho(t))e^{j\Phi(\rho(t))}$ is the complex soft envelop of the amplified signal $y(t)$. The SSPA model is usually modeled using Rapp's model as [24]

$$\begin{aligned} A\left[\rho(t)\right] &= \frac{\rho(t)}{\left[1+\left(\frac{\rho(t)}{x_{sat}}\right)^{2p}\right]^{\frac{1}{2p}}} \\ \Phi\left[\theta(t)\right] &= 0 \end{aligned} \tag{5}$$

where x_{sat} sets the output saturation level, and p is the parameter that controls the AM/AM sharpness of the saturation region, as shown in Fig. 1. The AM/AM characteristics become similar to that of the soft limiter as $p \to \infty$.

Alternatively, the nonlinear HPA output signal $y(t)$ can be modeled as [20]

$$y(t) = K_0 x(t) + d(t) \tag{6}$$

where $x(t)$ is the input signal, K_0 is a constant complex gain, and $d(t)$ is additive zero-mean noise with variance σ_d^2. (The reader is referred to [20] and [21] for more on K_0 and $d(t)$.)

It is usually undesirable to operate the HPA in the saturation region, and hence, the operating point of an HPA is lowered by certain input backoff (IBO). The IBO is the ratio of the saturation power of the HPA and the average power of the input signal, which is given by

$$\mathrm{IBO_{dB}} = 10\log_{10}\left(\frac{P_{sat}}{P_{av}}\right) \tag{7}$$

where P_{sat} and P_{av} are the saturation power of the HPA and the average power of the output signal, respectively.

C. BER Metric

The demodulated symbol on the subcarrier n of the received OFDM signal, considering nonlinearly amplified signal through a radio channel, is given by

$$z_n = K_0 H_n\left(x_n\right) + H_n d_n + w_n \tag{8}$$

where H_n indicates the channel frequency response corresponding to subcarrier n, and w_n is the additive white Gaussian noise (AWGN) with variance $\sigma_w^2 = P_{\mathrm{out}} N_0/(E_b \log_2 M)$ (E_b is the energy per bit at the output of the HPA, N_o is the one-sided noise spectral density, and P_{out} is the signal mean power at the output of HPA).

Assuming perfect knowledge of channel state information and K_0 and with the zero forcing (ZF) equalizer applied at the receiver, the instantaneous signal-to-noise ratio (SNR) can be described as

$$\gamma = \gamma_c \frac{\alpha}{\alpha\sigma_d^2 + \sigma_w^2} \tag{9}$$

where $\gamma_c = |K_0|^2\sigma_x^2$ (σ_x^2 is the variance of input signal), and $\alpha = |H|^2$ is the fading channel power. Its probability density function $f_\gamma(\gamma)$ is expressed as [21]

$$f_\gamma(\gamma) = \begin{cases} \frac{\gamma_c \sigma_w^2}{\Omega\left(\gamma_c - \sigma_d^2\gamma\right)^2} e^{\frac{-\gamma\sigma_w^2}{\Omega\left(\gamma_c - \sigma_d^2\gamma\right)}}, & \text{if } 0 \le \gamma < \frac{\gamma_c}{\sigma_d^2} \\ 0, & \text{otherwise} \end{cases} \tag{10}$$

where $\Omega = \mathbb{E}[\alpha]$ is an average fading power.

According to [21], the BER of an uncoded OFDM M-QAM signal over a quasi-static frequency-flat Rayleigh channel, P_b^R is given by

$$P_b^R = \int_0^{\frac{\gamma_c}{\sigma_d^2}} P_b^A(\gamma) f_\gamma(\gamma) d\gamma \tag{11}$$

where $p_b^A(\gamma)$ is the BER of the OFDM M-QAM signal in the AWGN channel,[1] which is expressed as [21]

$$P_b^A(\gamma) = a \cdot \mathrm{erfc}(\sqrt{b\gamma}) \tag{12}$$

where $\mathrm{erfc}(\cdot)$ is the complementary Gaussian error function, and $a = (2(\sqrt{M}-1))/(\sqrt{M}\log_2(M))$ and $b = (3\log_2(M))/(M-1)$ for M-QAM. The solution to (11) is given in [22].

III. Phase Realignment-Based Peak-to-Average Power Ratio Reduction Techniques

Here, we propose a simple nonbijective[2] constellation mapping technique of PAPR reduction based on the realignment of the phase of the CF constellation points, namely, PR and MPR. The PR has been introduced in our previous work [12]. Furthermore, we generalize our proposed technique, i.e., MPR, for the HOM using M-QAM and propose four types of MPR

[1]For the AWGN channel, γ can be calculated using (9) with $\alpha = 1$.

[2]Mapping is done without using one-to-one transformation to form the desired output.

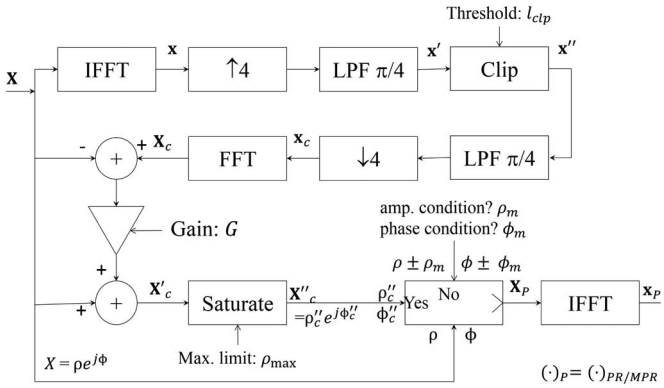

Fig. 2. Implementation of the PR/MPR in the OFDM system.

constellation structures to enhance the PAPR reduction with predefined transmit EVM.

The PR and MPR are implemented right after CF and fast Fourier transform (FFT) operation in the frequency domain, as shown in Fig. 2. As shown in the figure, the proposed techniques produce a time-domain signal $\mathbf{x}_p$ (represents either $\mathbf{x}_{\mathrm{PR}}$ or $\mathbf{x}_{\mathrm{MPR}}$) that replaces the original signal $\mathbf{x} = [x_0, x_1, \ldots, x_{N-1}]$ obtained by the IFFT on a set of frequency-domain values $\mathbf{X} = [X_0, X_1, \ldots, X_{N-1}]$. $\mathbf{x}$ is oversampled with the oversampling factor of L and filtered to obtain $\mathbf{x}' = [x'_0, x'_1, \ldots, x'_{NL-1}]$ before clipping operation. The clipping operation is defined as follows:

$$x''_k = \begin{cases} x'_k, & \text{if } \|x'_k\| \le l_{clp} \\ l_{clp}\frac{x'_k}{\|x'_k\|}, & \text{otherwise} \end{cases} \tag{13}$$

where $\mathbf{x}'' = [x''_0, x''_1, \ldots, x''_{NL-1}]$ is the clipped signal, and $l_{clp} = \sqrt{\mathrm{CR} \cdot P_{av}}$ is the clipping threshold obtained by using clipping ratio CR and the average power. Filtering, downsampling, and FFT are performed to obtain the CF signal in the frequency domain, i.e., $\mathbf{X}_c$, which is further processed as

$$\mathbf{X}'_c = \mathbf{X} + G(\mathbf{X}_c - \mathbf{X}) \tag{14}$$

where $\mathbf{X}_c - \mathbf{X}$ is the CF noise (error vectors), and G is the parameter to set the intensity of CF noise.

Now, the saturation operation is implemented on $\mathbf{X}'_c$ with the maximum amplitude threshold $\rho_{\max}$ to obtain $\mathbf{X}''_c = \boldsymbol{\rho}''_c e^{-j\boldsymbol{\phi}''_c}$ that avoids an excessive growth of the amplitude. Then, the conditions on the amplitude and phase of the CF constellation are imposed to obtain either the PR or the MPR signal. In what follows, we describe such conditions for the PR and MPR, respectively.

A. PR

The idea of PR can be easily explained for flat power lying in each quadrant of the complex plane equidistant from the real and the imaginary axis. An error occurs when the noise causes the received sample to fall into one of the other three quadrants. The error rate can be decreased by increasing the distance of the constellation point from the decision boundary, which, in turn, increases the transmission power for the data block as in the ACE. The PAPR is reduced at the cost of increased power, and this would be a serious drawback in a practical scenario.

Here, we introduce the idea of balancing the Euclidean distance of the CF signal from the decision boundary without significantly increasing the transmitted power of the data block while reducing the PAPR adequately. In PR, the phase and the amplitude of the distorted signals are manipulated to achieve the low-PAPR profile. The price paid is a slight degradation of the BER performance, which often could be compensated, as discussed in [23], i.e., that PAPR reduction would improve both the spectral and the energy efficiency. Clearly, both the amplitude and phase play a critical role in the PAPR of a signal. The high peak is obtained when the instantaneous amplitudes of the N exponential signals (with different frequencies and phase shifts) have peaks aligned at the same time. The PAPR of the CF signal is low at a price of highly degraded BER performance. Careful restriction of the amplitude and phase of the CF signal to improve its BER performance would retain much of the signal property that contributes to low PAPR. Following (14) and saturation operation, the phase $\boldsymbol{\phi}''_c = [\phi''_c(1), \phi''_c(2), \ldots, \phi''_c(N-1)]$ is realigned to its original state as was prior to CF, and the amplitude beyond the range of $\pm\rho_m$ from the original amplitude is scaled to the respective margin. It is to be noted that, for the four outermost-corner constellation points, there is no restriction on the outward-extending constellation, as it has already been dealt with. Thus, for 4-QAM (as well as for M-PSK), there is only a lower margin $\rho - \rho_m$ active, whereas for higher-order M-QAM ($M = 16, 64, 256, \ldots$), there is an additional active upper margin $\rho + \rho_m$ except for the outermost (corners and sides) constellation points. Consider the polar representation of the input M-QAM modulated symbol $\mathbf{X} = \rho e^{-j\phi}$, where $\rho = [\rho(1), \rho(2), \ldots, \rho(N-1)]$ and $\phi = [\phi(1), \phi(2), \ldots, \phi(N-1)]$ are the amplitude and phase of $\mathbf{X}$. Then, the condition imposed on amplitude and phase can be mathematically expressed, respectively, as

$$\rho_{\mathrm{PR}}(n) = \begin{cases} \rho(n) + \rho_m, & \text{if } \rho''_c(n) > \rho(n) + \rho_m \\ \rho(n) - \rho_m, & \text{if } \rho''_c(n) < \rho(n) - \rho_m \\ \rho''_c(n), & \text{otherwise} \end{cases} \tag{15}$$

$$\phi_{\mathrm{PR}}(n) = \phi(n) \tag{16}$$

where ρ_{PR} and ϕ_{PR} are the amplitude and the phase vectors of the PR signal.

Thus, the PR signal in the time domain $\mathbf{x}_{\mathrm{PR}}$ can be obtained by using IFFT on $\mathbf{X}_{\mathrm{PR}} = \rho_{\mathrm{PR}} e^{-j\phi_{\mathrm{PR}}}$.

The conceptual process of the PR is shown in Fig. 3, which shows the constellation points in the first quadrant of 4-QAM before and after implementing the CF and PR. The dashed arc represents the amplitude margin and the maximum amplitude threshold. The arrows indicate the direction in which the CF constellation point is shifted as the PR process is carried out. All constellation points having their amplitudes within the amplitude margin from the conventional point are left unchanged, whereas the remaining constellation points undergo amplitude scaling into the boundary defined by the amplitude margin.

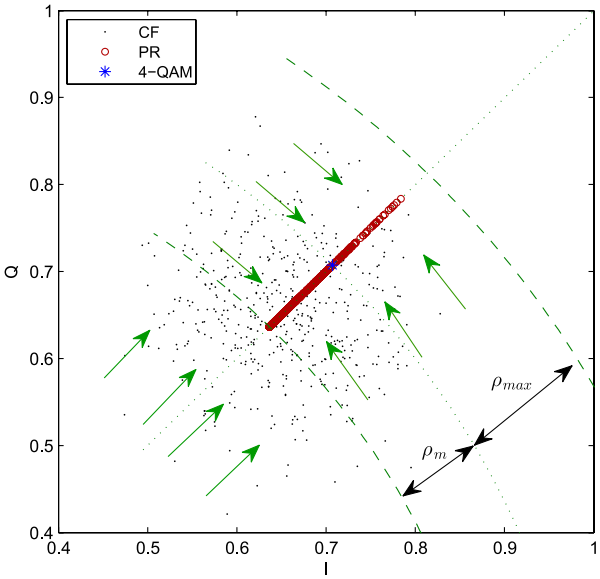

Fig. 3. Conceptual process of PR in the first quadrant of 4-QAM constellation.

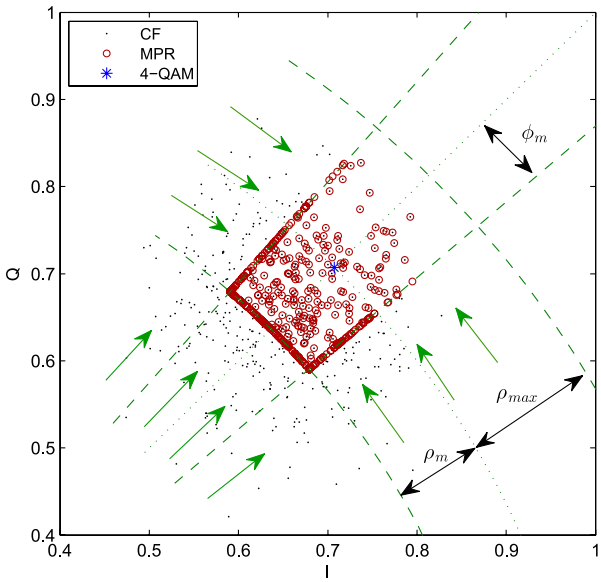

Fig. 4. Conceptual process of MPR in the first quadrant of 4-QAM constellation.

B. MPR

The underlying principle of the PR is the controlled increment of the Euclidean distance of the CF constellation points to achieve PAPR reduction. Realigning the phase not only enhances the BER performance compared with the CF but also regenerates peaks to increase the PAPR slightly. This can be solved by introducing a phase margin ϕ_m in addition to the amplitude margin ρ_m. Such a phase margin also allows an optimal tradeoff between the PAPR and the BER performance. The introduction of the phase margin to the PR process gives rise to the MPR. Setting an optimal phase margin for a given transmit EVM would further help retain much of the low-PAPR property of the CF signal.

In MPR, the phases of those CF constellation points residing inside the allowable phase $(\phi \pm \phi_m)$ are left unchanged, and those of the remaining constellation points would be changed to the respective phase boundary. This can be mathematically represented as

$$\phi_{\mathrm{MPR}}(n) = \begin{cases} \phi(n) + \phi_m, & \text{if } \phi_c''(n) > \phi(n) + \phi_m \\ \phi(n) - \phi_m, & \text{if } \phi_c''(n) < \phi(n) - \phi_m \\ \phi_c''(n), & \text{otherwise} \end{cases} \quad (17)$$

where ρ_{MPR} and ϕ_{MPR} are the amplitude and phase vectors of the MPR signal.

The concept of the MPR process is shown in Fig. 4. The MPR process is similar to the PR process except that the phase of the CF constellation is limited by the phase margin $(\pm\phi_m)$ along with the amplitude margin.

The resulting constellations by implementing the PR and MPR are shown in Fig. 5 for 4-QAM and 16-QAM.

C. Types of MPR Constellation

The performance in terms of both the BER and PAPR would vary as we restrict the phase of the CF signal in the

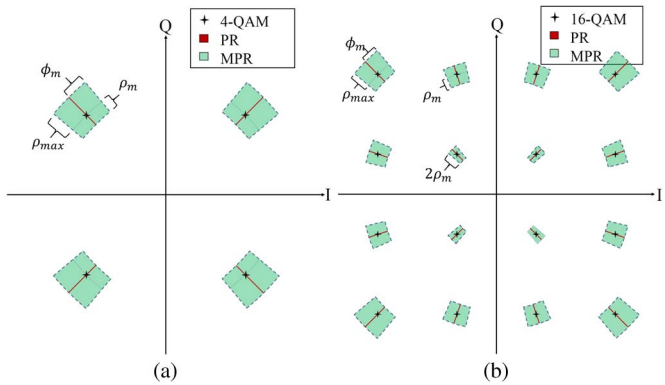

Fig. 5. Signal constellations after applying PR and MPR techniques. (a) 4-QAM. (b) 16-QAM.

MPR. In the HOM such as M-QAM $(M = 16, 64, 256, \ldots)$, the constellation points can be classified into three categories: 1) outer-corner constellation points; 2) side constellation points; and 3) inner constellation points. The inner constellation points have limited room to extend its amplitude and phase and, hence, are highly prone to error. The side constellation points are less prone to error, whereas the corner constellation points are least prone to error. Thus, varying the intensity of CF noise (error vectors) in the inner constellation points would result in a significant difference in the BER performance. This phenomenon is also true for the side constellation points but has a lower impact. Based on this, we propose four possible variations in the structure of the MPR constellation in an attempt to trade off the BER degradation and PAPR reduction in MPR. The MPR structures are shown in Fig. 6.

These MPR constellation structures in Fig. 6 can be obtained by means of amplitude scaling in (16) and controlled phase restriction. MPR_1 is the same as in (17). In MPR_2, the phase of the corner constellation points is restricted using (17), and those of the remaining constellation points are restricted by

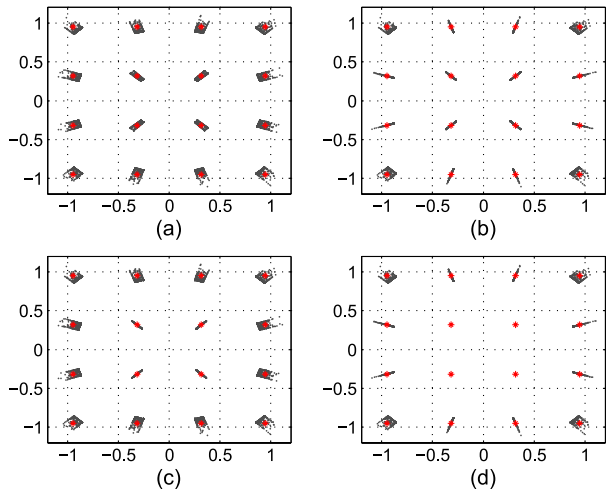

Fig. 6. MPR constellation structures for HOM illustrated using 16-QAM (a) MPR_1, (b) MPR_2, (c) MPR_3, and (d) MPR_4.

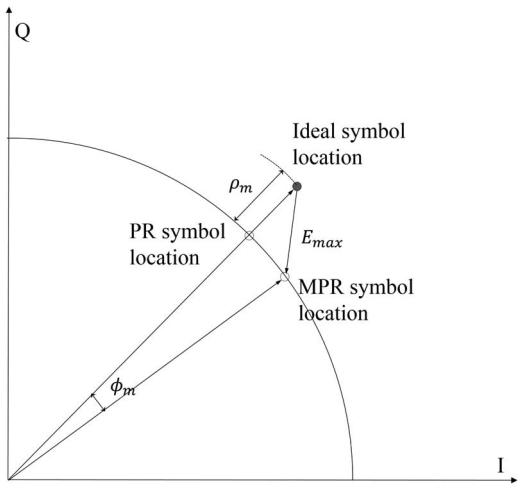

Fig. 7. Graphical representation of the error vector by implementing the PR/MPR.

using (15). In MPR_3, only the inner constellation points are restricted by using (15), and the remaining constellation points are restricted by using (17). Whereas, for MPR_4, the inner constellation points are kept the same as those of a conventional M-QAM constellation, the four outer-corner constellation points are restricted by using (17), and the remaining constellation points are restricted by using (15).

It is noted that although the maximum transmit EVM of these four types of MPR might be similarly designed, the BER performance of each might be unique. For instance, MPR_4 alters only the outer constellation points, which will have a significant difference in the PAPR and BER performance particularly for the HOM. Meanwhile, the BER performance of different types of MPR might be different when the effect of HPA is considered. It is worthwhile to study such an effect of different types of MPRs.

D. Amplitude Margin and Phase Margin

The next issue here is to determine the amplitude margin (ρ_m) and the phase margin (ϕ_m). Both the amplitude and phase margins are to be carefully chosen as the PAPR reduction and the BER performance of the proposed techniques depend on them.

As previously discussed, the PR/MPR generates distortion in the conventionally modulated symbols. The error vectors (for each subcarrier) that are generated by implementing the PR/MPR can be denoted as

$$\mathbf{E} = \mathbf{X}_{\text{PR/MPR}} - \mathbf{X} \tag{18}$$

where $\mathbf{E} = [E_0, E_1, \ldots, E_{N-1}]$. The EVM metric is a figure of merit for modulation accuracy, which can be obtained as

$$\text{EVM}\left(\mathbf{x}_{\text{PR/MPR}}\right)[\%] = \frac{1}{S_{\max}}\sqrt{\frac{\mathbf{E}\mathbf{E}^H}{N}} \tag{19}$$

where $S_{\max}$ is the maximum amplitude of the constellation.

Our objective here is to reduce the PAPR such that the transmit EVM of the PR/MPR constellation shall be less than the predefined threshold compared with the original modulated signal. In constraint clipping [14], the constraints appear to have no use upon optimization of the clipping level. This is due to the fact that the constraints limit the error vector within a specified amplitude margin around the original constellation points, where the error vectors have a Gaussian distribution. In contrast, the proposed technique has margins defined in terms of amplitude and phase, and thus, it is unique. The optimization problem to determine appropriate ρ_m and ϕ_m can be mathematically represented as

$$\min_{\rho_m,\phi_m} \max_{n} \left|\mathbf{x}_{\text{PR/MPR}}\left(\frac{n}{L}\right)\right|^2$$
$$\text{subject to EVM}\left(\mathbf{x}_{\text{PR/MPR}}\right)[\%] \leq \epsilon[\%] \tag{20}$$

where ϵ is the EMV threshold (in %).[3]

The problem in (20) requires the solution for the optimal combination of the amplitude and phase margins (ρ_m, ϕ_m), which makes it complex. To simplify (20), we can replace the constraint by

$$\text{EVM}_{\max}(\mathbf{x}_{\text{PR/MPR}})[\%] = \epsilon[\%] \tag{21}$$

where $\text{EVM}_{\max}$ is the maximum EVM.

The maximum error vector $E_{\max}$ caused by implementing the PR/MPR can be represented in terms of maximum magnitude and phase error that are analogous to ρ_m and ϕ_m, respectively, as shown in Fig. 7, and can be expressed as (by using small-angle approximation)

$$E_{\max} = \sqrt{\rho_m^2 + \phi_m^2}. \tag{22}$$

[3]Most modern digital communication standards have a predefined EVM threshold.

Thus, using (21) and (22), the problem in (20) can be simplified to a single-variable optimization problem as

$$\min_{\phi_m} \max_{n} \left|\mathbf{x}_{\mathrm{PR/MPR}}\left(\frac{n}{L}\right)\right|^2$$
$$\text{subject to } \rho_m = \sqrt{\left(\frac{\epsilon \cdot S_{\max}}{100}\right)^2 - \phi_m^2}$$
$$0 \le \phi_m \le \frac{\epsilon \cdot S_{\max}}{100}. \tag{23}$$

The problem in (23) can be easily solved numerically by using a technique such as the random search. The problem is readily solved for the PR by using $\phi_m = 0$. It is to be noted that the optimum margins are to be obtained only once for a given system. For MPRs, the problem may be solved by using random search, which has the complexity of $O(\log R)$, where R is the number of possible phase margins involved in the search.

E. PR/MPR Algorithm

The optimum margins for PR and each type of MPR are obtained once, as discussed in Section III-D. The proposed techniques of PAPR reduction can be summarized in algorithmic form as follows.

1) Starting with the data symbols in $\mathbf{X}$, apply oversampling and IFFT to obtain $\mathbf{x}'$.
2) Perform clipping using (13).
3) Perform filtering, downsampling, and FFT to obtain $\mathbf{X}_c$.
4) Obtain $\mathbf{X}_c'$ using (14).
5) Impose the condition on the maximum amplitude to obtain $\mathbf{X}_c''$.
6) Impose conditions on the amplitude and phase of $\mathbf{X}_c''$ to obtain $\mathbf{X}_{\mathrm{PR/MPR}}$. Such conditions are described in Section III-A–C.
7) Apply FFT on $\mathbf{X}_{\mathrm{PR/MPR}}$ to obtain $\mathbf{x}_{\mathrm{PR/MPR}}$.

F. Computational Complexity

The computational complexity is measured by the number of real multiplications (RM) and real additions (RA). The PR and MPR include extra IFFT and FFT operations, the CF operation, and the processing of the signal to impose the amplitude and phase conditions on the CF signal. By referring division as multiplication and subtraction as addition, the N-point radix-2 decimation-in-time IFFT or FFT implementation requires $2N\log_2(N)$ RM and $3N\log_2(N)$ RA [18]. It is considered that each complex multiplication requires four RM and two RA and that each complex addition requires two RA. For the CF operation, approximately $4NL + 2N$ RM and RA are required [18], where L is the oversampling factor.

For the PR/MPR, the CF signal needs to be converted into polar form and compared with amplitude and phase margins. Calculating the amplitude of N complex-valued samples requires $3N$ RM and N RA, and the phase requires approximately $2N$ RM. The comparison with each margins requires N subtractions. Hence, the proposed techniques require computation complexity that is equivalent to $4N\log_2(N) + 4NL + 7N$ RM and $6N\log_2(N) + 4NL + 5N$ RA.

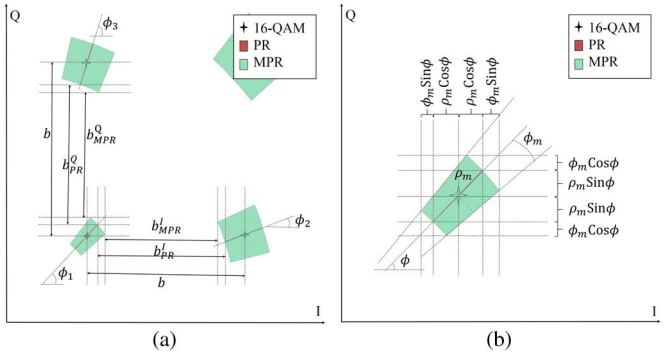

Fig. 8. Computation of the minimum Euclidean distance of the PR and the MPR applied constellation (the first quadrant of 16-QAM). (a) Euclidean distance along the in-phase and quadrature-phase axis. (b) Calculation of the maximum deviation from the conventional 16-QAM constellation.

IV. Bit Error Rate Analysis

Our proposed PR and MPR techniques could reduce the PAPR at the cost of slight BER degradation by allowing a certain amount of the transmit EVM, where some of the Euclidean distances are reduced as compared with those of the conventional signal constellation. Such constellation points will be assigned within the amplitude margin ρ_m and phase margin ϕ_m, and it will be reasonable to derive the upper-bound BER for the approximate average BER by evaluating the corresponding minimum Euclidean distance.

The minimum Euclidean distance in the PR and MPR applied constellations can be computed with the help of small-angle approximation. To demonstrate this, in Fig. 8, we consider the first-quadrant inner-constellation point of 16-QAM in Fig. 5(b). Fig. 8(a) shows the minimum Euclidean distance for conventional QAM, PR, and MPR along the in-phase and quadrature phase, and Fig. 8(b) shows the extension of the first-quadrant inner-constellation 16-QAM signal with the PR and MPR applied. It can be seen that the maximum constellation extension is present on either edge in the PR and on each of the four corners in the MPR. In the figure, it is shown that the maximum extension accounts for the minimum distance from the decision boundary and, thus, the minimum Euclidean distance. If ϕ is the phase of the conventional constellation points, the distance to the edges in PR and corners in MPR can be easily calculated using small-angle approximation, as shown in Fig. 8(b). The minimum Euclidean distance in the PR and MPR can be expressed as

$$b_{\mathrm{PR}} = b - \rho_m \max\left(\sum_{i=1}^{2}\cos\phi_i, \sum_{j=1}^{2}\sin\phi_j\right) \tag{24}$$

$$b_{\mathrm{MPR}} = b_{\mathrm{PR}} - \phi_m \max\left(\sum_{j=1}^{2}\cos\phi_j, \sum_{i=1}^{2}\sin\phi_i\right) \tag{25}$$

where $i, j \in [1, 2]$ indicate the neighboring constellation points sharing the decision boundary along the in-phase and the quadrature phase, respectively.

Thus, substituting b_{PR} and b_{MPR} in (24) and (25) for b in (11), we can easily get the upper bound BER of the PR and MPR applied scheme, respectively.

TABLE I
SIMULATION PARAMETERS

Parameter	Value
Bandwidth	8 MHz
Total number of subcarriers (FFT size) N	8192
CR for CF	(5.3, 6.5, 7.1) dB
IBO	(6, 7, 9) dB
Modulation	M-QAM; M = 16, 64, and 256
Channel model	Rayleigh fading
Power amplifier model	Soft limiter and Rapp's model ($p = 3$)
#. Monte Carlo (MC)	10^6

V. NUMERICAL RESULTS

Here, we first obtain the optimal amplitude and phase margins (ρ_m, ϕ_m) numerically and then evaluate the PAPR and BER performance of the proposed PR and MPR in comparison with the various existing PAPR reduction techniques, namely, PTS, SLM, and ACE. The phase rotation factor for both the PTS and SLM is chosen from $\{+1, -1, +j, -j\}$. The number of subblocks for the PTS is $V = 4$, and the number of candidate data blocks for SLM is $C = 8$. For the ACE,[4] we consider the algorithm adopted in the DBV-T2 system, which is available in [19].

We consider an OFDM system with 8192 subcarriers and 8-MHz bandwidth. For the HPA model, we apply the soft limiter and Rapp's models. Our simulation parameters are listed in Table I. While the complexity of the proposed PR/MPR is evaluated in Section III-F, we evaluate the PAPR performance, the BER performance, and the OOB radiation as follows. For a fair comparison, we consider normalizing all the systems to the unit energy, unless otherwise mentioned.

A. Optimization of the Margins

The choice of the amplitude and phase margins determines the performance of the proposed PAPR reduction techniques. Here, we determine such margins to satisfy (23) via numerical simulation.

For PR, the optimum margin ρ_m can be readily obtained by putting $\phi_m = 0$ in (23). For MPR, we obtain the PAPR for various phase margins, i.e., ϕ_m°.[5] Fig. 9 shows the PAPR reduction against the phase margins (ϕ_m°) for four types of MPR in the OFDM 16-, 64-, and 256-QAM systems, respectively. The optimal PAPR reduction is indicated for each case. The EVM threshold ϵ values were assigned as 5%, 1.7%, and 0.9% for 16-, 64-, and 256-QAM, respectively.

The optimum amplitude and phase margins for the PR and MPRs along with their PAPR reduction in 16-, 64-, and 256-QAM are listed in Table II. The optimum amplitude margin is calculated using the first constraint of the problem in (23).

B. PAPR Performance

The CCDFs of the proposed techniques are compared with those of the ACE, PTS, and SLM. The CCDF plots of the proposed PR and MPR techniques along with others are shown in Figs. 10–12 for 16-, 64-, and 256-QAM, respectively. It is shown that the CCDFs of all the proposed techniques are consistently better than ACE for all modulation orders. The CCDFs of MPR_1 and MPR_3 are much better compared with those of PTS and SLM for 16-QAM. However, as the modulation order increases, the PAPR performance degrades for the proposed techniques, whereas the PTS and SLM have constant reduction. For instance, for 64-QAM, the CCDF of $1e-1$, MPR_1 performs better than the PTS, and MPR_3 performs better than the SLM; such tendency reverses as the CCDF decreases to $1e-2$, as shown in Fig. 11. This is because the proposed techniques are based on the shaping of the CF in the frequency domain for a given CR. When the modulation order increases, the CR should be increased as the EVM threshold needs to be decreased. Upon increasing the CR and decreasing ϵ, there is only little room for the CF-noise-shaping-based PAPR reduction techniques to improve the PAPR.

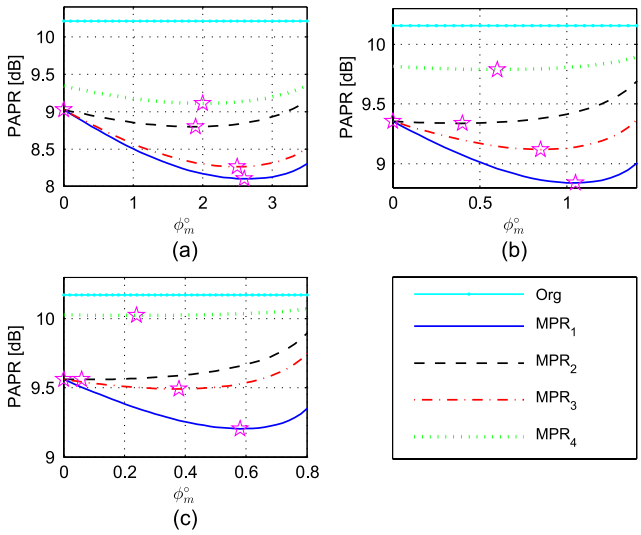

Fig. 9. PAPR versus ϕ_m° $(\rho_m = f(\epsilon, \phi_m^\circ))$ for different types of MPR in the OFDM M-QAM system. (a) $M = 16$, CR = 5.3 dB; (b) $M = 64$, CR = 6.5 dB; and (c) $M = 256$, CR = 7.1 dB.

We consider the OFDM 16-QAM to further illustrate the peak reduction of the OFDM signals achieved by the PR $(\rho_m = 0.0671)$ and the MPR $(\rho_m = 0.0494,\ \phi_m^\circ = 2.6^\circ)$. Fig. 13 shows the amplitudes of the PR, MPR, CF, and ACE applied OFDM signals along with the original OFDM signal, with the PAPR (instantaneous) of 9.23, 8.29, 5.47, 10, and 10.4 dB, respectively. The PR, MPR, CF, and ACE provide PAPR reduction of 1.17, 2.11, 4.93, and 0.4 dB, respectively. In the PR, MPR, and CF, the average power reduction values are 0.16, 0.14, and 0.17 dB, respectively, whereas the average power reduction actually increases by 0.05 dB in the ACE. Note that the results in Fig. 13 are obtained without power normalization.

MPR_1 performs the best, followed by MPR_3, PR, and MPR_2, whereas MPR_4 performs slightly better than the ACE. For 64-QAM and 256-QAM, MPR_2 and MPR_3 are close to the PR in terms of the CCDF. This reflects the fact that the inner-constellation structure remains the same for them, and as the modulation order increases, the difference among them

[4]Parameter G is set to 1 in this paper since the average power is minimum for the ACE at $G = 1$ (see [19] for more).

[5]ϕ_m° is the phase margin in degrees ($\phi_m = \phi_m^\circ \pi/180$).

TABLE II
OPTIMUM AMPLITUDE AND PHASE MARGINS FOR M-QAM WITH $M = 16$, 64, AND 256

Modulation	CR	ϵ	PR (ρ_m)	MPR$_1$ (ρ_m, ϕ_m°)	MPR$_2$ (ρ_m, ϕ_m°)	MPR$_3$ (ρ_m, ϕ_m°)	MPR$_4$ (ρ_m, ϕ_m°)
16-QAM	5.3 dB	5%	0.0671	(0.0494, 2.6)	(0.0583, 1.9)	(0.0510, 2.5)	(0.0573,2)
PAPR reduction			1.185 dB	2.11 dB	1.412 dB	1.947 dB	1.1 dB
64-QAM	6.5 dB	1.7%	0.0260	(0.0184, 1.05)	(0.0250, 0.4)	(0.0213, 0.85)	(0.0238, 0.6)
PAPR reduction			0.8 dB	1.316 dB	0.816 dB	1.036 dB	0.367 dB
256-QAM	7.1 dB	0.9%	0.0146	(0.0106, 0.58)	(0.0146, 0.06)	(0.0131, 0.38)	(0.0140, 0.24)
PAPR reduction			0.61 dB	0.966 dB	0.611 dB	0.679 dB	0.146 dB

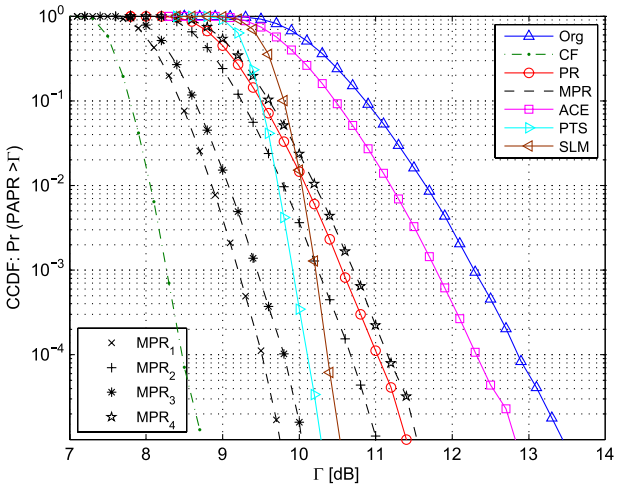

Fig. 10. CCDF of the PAPR for PR, MPR, and other techniques applied to the OFDM 16-QAM signal.

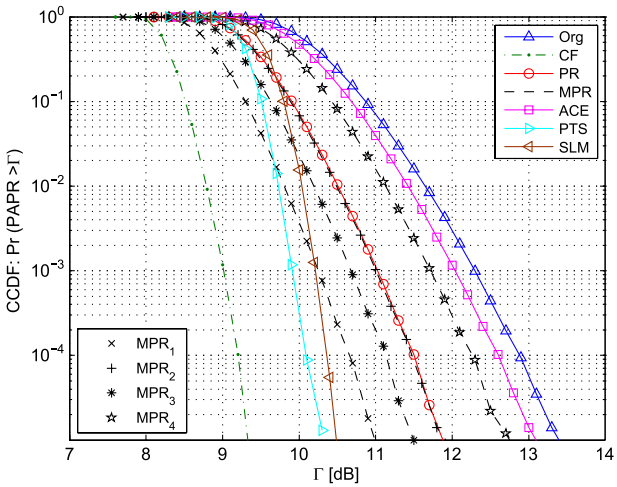

Fig. 11. CCDF of the PAPR for PR, MPR, and other techniques applied to the OFDM 64-QAM.

decreases. The ACE outer constellation extends further outward to achieve low PAPR. This causes many of the CF constellation points to contribute a large number of peak regrowth. In PR and MPR, many of the CF constellation points are left undamaged, and the amplitude and phase margins are designed such that there are inward extensions of the constellation as well, thereby decreasing the overall power. Thus, the PR and MPR have a higher PAPR reduction than the ACE.

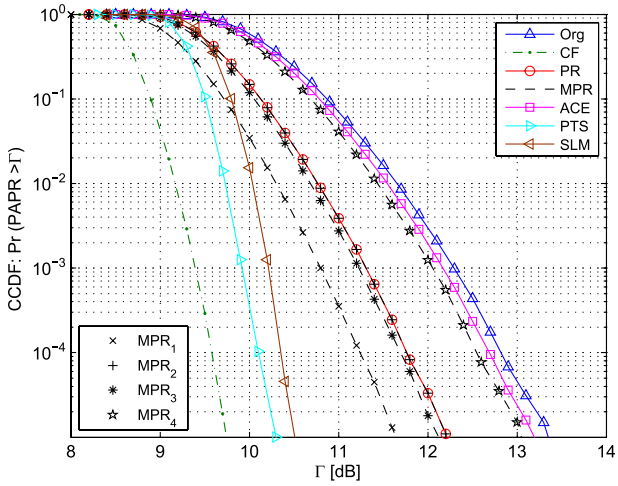

Fig. 12. CCDF of the PAPR for PR, MPR, and other techniques applied to the OFDM 256-QAM.

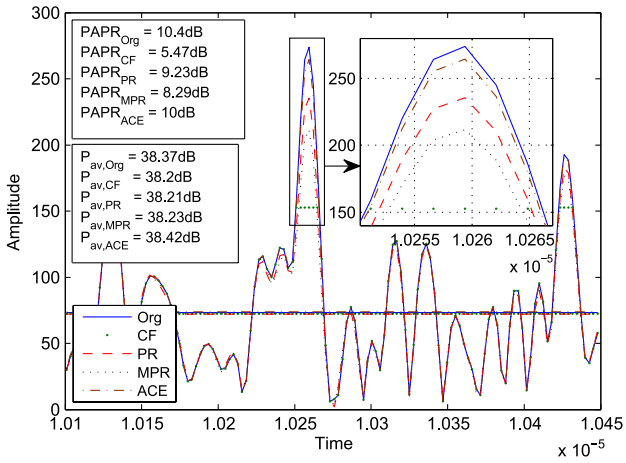

Fig. 13. Amplitudes of the OFDM 16-QAM signal with and without applying the CF, PR, MPR, and ACE.

TABLE III
APPROXIMATE PAPR REDUCTIONS (dB) ACHIEVED BY VARIOUS PAPR REDUCTION TECHNIQUES FOR CCDF OF $1e-3$

M-QAM	PR	MPR$_1$	MPR$_2$	MPR$_3$	MPR$_4$	ACE	PTS	SLM
16-QAM	1.7	3.1	2.1	2.9	1.6	0.5	2.4	2.1
64-QAM	1.3	2.05	1.35	1.7	0.6	0.3	2.4	2.1
256-QAM	1	1.6	1.1	1	0.3	0.15	2.4	2.1

Based on the results in Figs. 10–12, the approximate PAPR reductions achieved by the various techniques for the CCDF of $1e-3$ are listed in Table III.

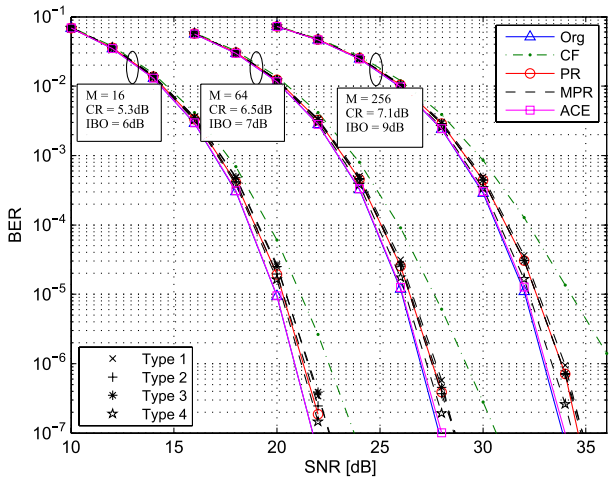

Fig. 14. BER performance of various PAPR reduction techniques in the OFDM 16-, 64-, and 256-QAM with the soft limiter PA model under the Rayleigh fading channel (ZF equalizer).

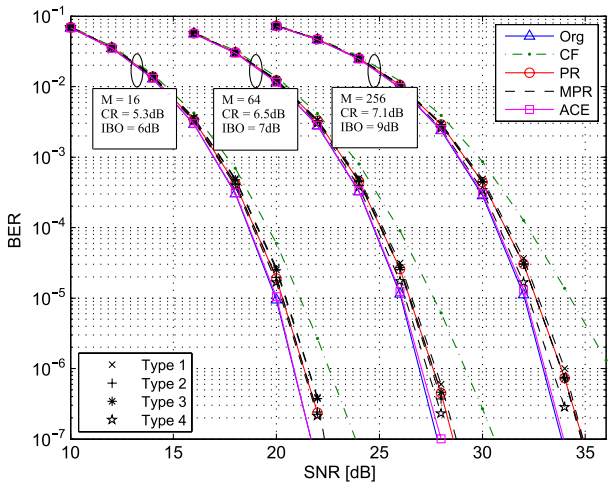

Fig. 15. BER performance of various PAPR reduction techniques in the OFDM 16-, 64-, and 256-QAM with Rapp's HPA model ($p = 3$) under the Rayleigh fading channel (ZF equalizer).

C. BER Performance

The BER performance of the proposed techniques and the ACE applied to the OFDM 16-QAM, 64-QAM, and 256-QAM systems are analyzed in conjunction with the nonlinear HPA over the Rayleigh fading channel. These plots are shown in Figs. 14 and 15 for the soft limiter model and Rapp's model of HPA, respectively, where it is observed that all the proposed techniques perform within 0.5 and 0.8 dB of SNR loss for the soft limiter model and Rapp's model of HPA, respectively. It is also observed that the BER degradation is not quite sensitive to the nonlinearity of HPA for all the proposed techniques, mainly because of the choice of the IBO values. The BER degradation in the proposed techniques can be limited by reducing the EVM threshold (ϵ). Furthermore, we can observe that with the SNR loss of up to 0.8 dB, to achieve the same BER performance as that of the conventional OFDM, the proposed techniques can achieve the PAPR reduction of up to 3.1 dB, even when the nonlinearity is present in the HPA.

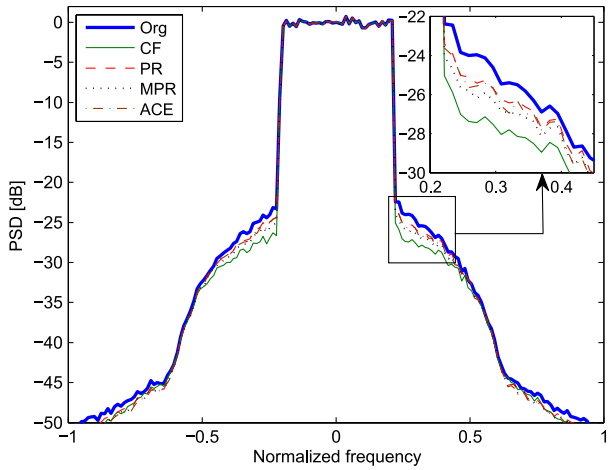

Fig. 16. Power spectrum density of various PAPR reduction techniques in the OFDM 16-QAM with Rapp's HPA model ($p = 3$).

D. OOB Radiation

The spectra of the proposed techniques are compared with that of the ACE and the original OFDM signal. Fig. 16 shows the power spectrum density plots for these techniques. The figure shows that the OOB of both the PR and MPR is lower than the original OFDM signal. The OOB of the PR is similar to that of the ACE, whereas the MPR has lower OOB radiation. On the other hand, the CF OFDM signal has the lowest OOB radiation. This is because the shaping of the CF noise in the PR, MPR, and ACE causes OOB radiation to slightly increase.

VI. Conclusion

In this paper, new PAPR reduction techniques called PR and its modified version MPR have been proposed. Both the PR and the MPR are based on CF noise shaping in the frequency domain, where the PR allows the fluctuation of the amplitude of the CF constellation, and the MPR allows the fluctuation of both the amplitude and the phase of the CF constellation. Furthermore, four possible variations in the structure of the MPR constellation have been proposed. The PR and MPR techniques are designed to reduce the PAPR at reduced overall signal power while retaining the EVM to a predefined threshold.

Our simulation results demonstrate that all the proposed techniques would be effective in reducing PAPR by up to 3.1, 2.05, and 1.6 dB for the CCDF of $1e^{-3}$ with the transmit EVM [%] of less than 5%, 1.7%, and 0.9% for 16-, 64-, and 256-QAM, respectively. Such a condition on the transmit EVM causes the BER degradation that is equivalent to the SNR loss of up to 0.5 and 0.8 dB, respectively, for the soft limiter model and Rapp's model of HPA. The channel was assumed to be Rayleigh fading with a ZF equalizer employed at the receiver. MPR_1 performs the best among the proposed techniques, which outperforms the PTS and SLM for 16-QAM and performs comparable to the PTS and SLM for 64-QAM. In addition, the PTS and SLM have high complexity and may require side information to be transmitted. The complexity of the proposed

techniques is equivalent to that of SLM with two candidate data blocks. Thus, the proposed MPR_1 should be more effective in terms of PAPR reduction and implementation complexity, although there is certain predefined transmit EVM. On the other hand, the PR, MPR_2, and MPR_3, in general, have moderate PAPR reductions, whereas MPR_4 merely performs better than the ACE.

The PAPR reduction of the proposed techniques can be further improved by using an iterative approach as in the case of the ICF and the ACE, which would be our future research.

REFERENCES

[1] R. V. Nee and R. Prashad, *OFDM Wireless Multimedia Communication*. Boston, MA, USA: Artech House, 2000.

[2] M. O'Droma, N. Mgebrishvili, and A. Goacher, "Linearity and efficiency issues in RF power amplifiers for future broadband wireless access systems," in *Proc. URSI Gen. Assem.*, 2002, pp. 1–4.

[3] X. Li and L. J. Cimini, Jr., "Effects of clipping and filtering on the performance of OFDM," *IEEE Commun. Lett.*, vol. 2, no. 5, pp. 131–133, May 1998.

[4] X. Zhu, W. Pan, H. Li, and Y. Tang, "Simplified approach to optimized iterative clipping and filtering for PAPR reduction of OFDM signals," *IEEE Trans. Commun.*, vol. 61, no. 5, pp. 1891–1901, May 2013.

[5] H. B. Jeon, J. S. No, and D. J. Shin, "A new PAPR reduction scheme using effective peak cancellation for OFDM systems," *IEEE Trans. Broadcast.*, vol. 58, no. 4, pp. 619–628, Dec. 2012.

[6] L. Dan, T. Li, Y. Xiao, and S. Li, "Performance of peak cancellation for PAPR reduction in OFDM system," in *Proc. ICCCAS*, May 2008, pp. 283–287.

[7] C. Li, T. Jiang, Y. Zhou, and H. Li, "A novel constellation reshaping method for PAPR reduction of OFDM signals," *IEEE Trans. Signal Process.*, vol. 59, no. 6, pp. 2710–2719, Jun. 2011.

[8] L. Yang, K. K. Soo, S. Q. Li, and Y. M. Siu, "PAPR reduction using low complexity PTS to construct of OFDM signals without side information," *IEEE Trans. Broadcast.*, vol. 57, no. 2, pp. 284–290, Jun. 2011.

[9] H. B. Jeon, J. S. No, and D. J. Shin, "A low-complexity SLM scheme using additive mapping sequences for PAPR reduction of OFDM signals," *IEEE Trans. Broadcast.*, vol. 57, no. 4, pp. 866–875, Dec. 2011.

[10] J. C. Chen, M. H. Chiu, Y. S. Yang, and C. P. Li, "A suboptimal tone reservation algorithm based on cross-entropy method for PAPR reduction in OFDM systems," *IEEE Trans. Broadcast.*, vol. 57, no. 3, pp. 752–756, Sep. 2011.

[11] T. Jiang and G. Zhu, "Complement block coding for reduction in peak-to-average power ratio of OFDM signals," *IEEE Commun. Mag.*, vol. 43, no. 9, pp. S17–S22, Sep. 2005.

[12] R. Shrestha *et al.*, "PAPR reduction and Pre-distortion techniques against non-linear distortion of satellite WiBro," in *Proc. JC-SAT Conf.*, Busan, Korea, Nov. 2008, pp. 145–154.

[13] B. S. Krongold and D. L. Jones, "PAR reduction in OFDM via active constellation extension," *IEEE Trans. Broadcast.*, vol. 49, no. 3, pp. 258–268, Sep. 2003.

[14] R. J. Baxley, Z. Chunming, and G. T. Zhou, "Constrained clipping for crest factor reduction in OFDM," *IEEE Trans. Broadcast.*, vol. 52, no. 4, pp. 570–575, Dec. 2006.

[15] A. Mobasher and A. K. Khandani, "Integer-based constellation-shaping method for PAPR reduction in OFDM systems," *IEEE Trans. Commun.*, vol. 54, no. 1, pp. 119–127, Jan. 2006.

[16] M. Sharif, C. Florens, M. Fazel, and B. Hassibi, "Amplitude and sign adjustment for peak-to-average-power reduction," *IEEE Trans. Commun.*, vol. 53, no. 8, pp. 1243–1247, Aug. 2005.

[17] S. H. Han and J. H. Lee, "Peak-to-average power ratio reduction of an OFDM signal by signal set expansion," in *Proc. IEEE ICC*, Jun. 2004, vol. 2, pp. 867–871.

[18] Y. Rahmatallah and S. Mohan, "Peak-to-average power ratio reduction in OFDM systems: A survey and taxonomy," *IEEE Commun. Surveys Tuts.*, vol. 15, no. 4, pp. 1567–1592, 4th Quart. 2013.

[19] *Digital Video Broadcasting (DVB); Frame Structure Channel Coding and Modulation for a Second Generation Digital Terrestrial Television Broadcasting System (DVB-T2)*, ETSI EN 302 755 V1.2.1, 2011.

[20] D. Dardari, V. Tralli, and A. Vaccari, "A theoretical characterization of nonlinear distortion effects in OFDM systems," *IEEE Trans. Commun.*, vol. 40, no. 10, pp. 1755–1764, Oct. 2000.

[21] H. Bouhadda *et al.*, "Theoretical analysis of BER performance of nonlinearly amplified FBMC/OQAM and OFDM signals," *EURASIP J. Adv. Signal Process.*, vol. 2014, no. 1, p. 60, May 2014.

[22] R. Zayani, H. Shaiek, D. Roviras, and Y. Medjahdi, "Closed-form BER expression for (QAM or OQAM) based OFDM system with HPA nonlinearity over Rayleigh fading channel," *IEEE Wireless Commun. Lett.*, vol. 4, no. 1, pp. 38–41, Feb. 2015.

[23] T. Jiang, C. Li, and C. Ni, "Effect of PAPR reduction on spectrum and energy efficiencies in OFDM systems with class-A HPA over AWGN channel," *IEEE Trans. Broadcast.*, vol. 59, no. 3, pp. 513–519, Sep. 2013.

[24] C. Rapp, "Effects of the HAP-nonlinearity on a 4-DPSK/OFDM," in *Proc. 2nd ECSC*, Liege, Belgium, Oct. 1991, pp. 179–184.

Robin Shrestha received the B.E. degree in electronics and communication engineering from National College of Engineering, Tribhuvan University, Kathmandu, Nepal, in 2006; the M.E. degree in telecommunication engineering from the Department of Information and Telecommunication Engineering, Korea Aerospace University, Goyang, Korea, in 2009; and the Ph.D. degree in information and communication engineering from the Graduate School of IT and Telecommunication, Inha University, Incheon, Korea, in 2014.

He is currently a Postdoctoral Fellow with the Department of Electrical and Electronics Engineering, Yonsei University, Seoul, Korea. His research interests include orthogonal frequency-division multiplexing, filter-bank-based multicarrier modulation, peak-to-average power ratio, resource allocation, multiuser multiple-input multiple-output, and interference alignment.

Dr. Shrestha received the best Ph.D. graduate of 2014 spring award from the dean's office of the Graduate School of IT and Telecommunication, Inha University.

Jae Moung Kim (SM'13) received the B.S. degree from Hanyang University, Seoul, Korea, in 1974; the M.S.E.E. degree from the University of Southern California, Los Angeles, CA, USA, in 1981; and the Ph.D. degree from Yonsei University, Seoul, in 1987.

From September 1982 to March 2003, he was the Vice President of the Electronics and Telecommunications Research Institute (ETRI) for Radio and Broadcasting Technology Lab and the Executive Director of the Satellite Communications System Department with ETRI. Since then, he has been a Professor with the School of Information and Communication Engineering, Inha University, Incheon, Korea. He is the Director of the Wireless Transmission Laboratory (INHA-WiTLAB), working on next-generation wireless communications, including cognitive radio technologies. His research interests include telecommunications system modeling and performance analysis of broadband wireless systems, mobile communications, and satellite communications, particularly cognitive radio and mobile radio transmission technology for next generation.

Dr. Kim is the President of the Korea Society of Space Technology and an overseas member of the Institute of Electronics, Information, and Communication Engineers.

Jong-Soo Seo (F'14) received the B.S. degree in electronics engineering from Yonsei University, Seoul, Korea, in 1975 and the M.S. and Ph.D. degrees from the University of Ottawa, Ottawa, ON, Canada, in 1983 and 1988, respectively.

He was with International Datacasting Corporation and Canadian Astronautics Ltd., Canada, where he was engaged in research on digital satellite communications and data broadcasting systems for six years. Since 1995, he has been with the Department of Electrical and Electronic Engineering, Yonsei University, where he is currently a Professor. His current research interests include mobile multimedia broadcasting and beyond fourth-generation mobile radio systems.

Dr. Seo is an Associate Editor of the IEEE TRANSACTIONS ON BROADCASTING.